Energy Equip. Sys./ Vol. 12/No. 4/December 2024/ 455-477

ENERGY EQUIPSYS

Energy Equipment and Systems

www.energyequipsys.com

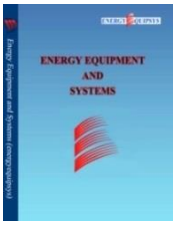

Integrated biomass and solar power-to-gas systems for energy storage and freshwater production: A 4E and multicriteria optimization approach

Manuscript Type
Research Paper

Authors

Shayan Rabet[a]
Ehsan Gholamian[a*]
Seyed Mohammad Seyed Mahmoudi[a]

[a]Department of Mechanical Engineering, University of Tabriz, Tabriz, Iran

Article history:

Received : 1 April 2024
Revised : 23 April 2024
Accepted : 29 April 2024

ABSTRACT

Today, rising concerns about energy shortages and environmental degradation have encouraged innovation in renewable energy sources and cutting-edge technology for capturing their full potential. The adoption of sustainable practices has resulted in the emergence of innovative cogeneration systems that incorporate municipal solid waste as a fuel source. By integrating advanced technologies—including digesters, organic Rankine cycles, multiple effect distillation, methanation, and proton exchange membranes—this system uniquely converts hydrogen and CO_2 into methane, enhancing fresh water production through heat recovery in the digestion process. We explore three multiobjective optimization employing machine learning and Greywolf algorithms to enhance system efficiency. The system has a significant CO_2 emission index of $0.1649 kg/kWh$ and total cost products of $12.91\ \$/GJ$, with a second-law thermodynamics efficiency of 32.07%. Strategic optimization is centered around the objective of increasing efficiency and net output power, while simultaneously reducing costs. This approach yields significant enhancements, including an exergy efficiency of 39.13% and a net output power of $30366.92\ KW$. Additionally, the product costs are lowered to $7.2571\ \$/GJ$. These results highlight the system's cost-effectiveness and alignment with sustainability principles, offering meaningful contributions to renewable energy technologies and environmental conservation.

Keywords: MED (Multiple Effect Distillation), CO_2 Capturing, PEME (Proton Exchange Membrane Electrolyzer), Digester, Methanation, Cogeneration, Multiobjective Optimization, Biogas.

1. Introduction

Over the past few years, concerns over environmental deterioration and energy shortages have pushed the shift towards renewable energy sources and the development of advanced technologies for their optimal use [1]. Utilizing digesters to transform municipal solid waste into energy is becoming more popular in this field as an effective method to reduce air and water pollution, as well as generate electricity. This methodology not only presents innovative strategies for waste management but also makes a substantial

* Corresponding author: Ehsan Gholamian
Department of Mechanical Engineering, University of Tabriz, Tabriz, Iran
Email: Eh.gholamian@tabrizu.ac.ir

contribution to carbon capture and the production of drinkable water [2]. In addition, the significance of Hydrogen as a vital energy transporter has received considerable focus, specifically regarding its production methods. One notable aspect is the generation of hydrogen using proton exchange membrane technology, which is well-known for its environmental friendliness and low maintenance needs [3]. The main objective in the development of carbon and hydrogen production systems is to utilize these gases for the synthesis of methane. The utilization of a reforming reactor for methane production is a remarkably efficient approach, providing the dual benefit of reducing greenhouse gas emissions and enhancing waste management practices. In order to show how these connected technologies might revolutionize how we deal with environmental problems and prepare the way for a more efficient and sustainable future, this essay attempts to do that in fact.

1.1. Literature review

Kim et al. [4] demonstrated that the utilization of supercritical CO_2 Rankine cycles, as opposed to conventional ORC, leads to improved efficiency in harnessing residual heat produced by gas turbines. The researchers investigated various S-CO_2 cycles, including simple, cascade, and split cycles. Their findings indicate that the split S-CO_2 cycle exhibits superior efficiency, characterized by lower exergy loss and higher system efficiency across a wide range of pressures and temperatures. This approach offers a more effective and uncomplicated alternative for recovering waste heat compared to traditional ORC systems. Ghasemzadeh et al. [5] analyzed a tri-generation system that integrates geothermal energy with an Organic Rankine Cycle (ORC), a double-effect absorption refrigeration system, and a humidification-dehumidification desalination unit. This setup aims to optimize the use of geothermal heat to simultaneously produce power, cooling, and freshwater. Initially, the system achieved an exergy efficiency of 44.2% and a product unit cost of 77.8 $/GJ. Through multi-objective optimization, these figures improved to 54% for exergy efficiency and 62.5 $/GJ for the cost, while power output increased to 180 kW. The study highlights significant efficiencies gained by integrating various energy recovery technologies in a single system. The integration of a digester with pyrolysis and combined heat and power (CHP) plants was proposed by Salman et al. [6] as a means to enhance biomethane production and improve energy efficiency in the valorization of municipal solid waste. The researchers attained a pyrolysis efficiency of 75% in isolation, which subsequently rose to 80% when integrated with a combined heat and power (CHP) facility. The inclusion of biochar derived from pyrolysis in the digester resulted in a comprehensive system efficiency of 79.7%, which exhibited a notable improvement compared to the combined utilization of pyrolysis and anaerobic digestion alone. Zhang et al. [7] added a digester and organic flash cycle to a novel flash-binary geothermal system and GT cycle, enhancing waste heat recovery for power and freshwater production. Their system achieved 35.43% exergetic efficiency, improving to 36.13% with triple-objective optimization, and a payback period reduced from 3.42 to 3.04 years. They also identified the highest exergy destruction in the combustion chamber and MSW digester, indicating key areas for efficiency improvements. Zeinali et al. [8] analyzed a sustainable electric power system utilizing a solar tower by day and syngas from municipal waste gasification by night. This hybrid setup, which includes air Brayton, reheat Rankine, and ORC, efficiently generates electricity across day and night cycles. Key findings indicate that turbine inlet temperature significantly influences system efficiency, with higher moisture in waste reducing syngas output and overall efficiency.

Behzadi et al. [9] explored a hybrid system combining a Photovoltaic/Thermal (PVT) unit, a PEM electrolyzer, and a double-effect absorption chiller, targeting enhanced hydrogen production and cooling. Their study identified significant inefficiencies, mainly in the PVT component, which accounted for the majority of exergy destruction, leading to an overall system exergy efficiency of about 10.56%. By optimizing operational temperatures, they demonstrated potential reductions in production costs, underscoring the importance of component integration and operational efficiency for improving both economic and environmental performance of renewable energy systems. Ni et al. [10] incorporated a

PEM electrolyzer within their thermodynamic-electrochemical framework for producing hydrogen, observing a simultaneous decline in both energy and exergy efficiencies as the current density rose. The findings reveal that the efficiencies are nearly identical and greatly influenced by the operational parameters of the electrolyzer, particularly the current density. The study provides important insights into improving the energy conversion efficiency of PEM electrolyzers.

Bailera et al. [11] explored the integration of Power to Gas (PtG) technology with electrochemical industries to enhance CO_2 utilization and energy storage. They suggested leveraging the hydrogen produced in electrochemical plants for methanation processes, thus bypassing the necessity for water electrolysis. This strategy is deemed both practical and financially sound, offering considerable prospects for reducing CO_2 emissions and augmenting energy storage capabilities. The research highlights the efficiency and environmental sustainability advantages of these combined systems. Desideri et al. [12] explored the incorporation of a CO_2 removal system into power plants, finding that although it is possible to achieve a 90% efficiency in CO_2 capture, this comes with substantial increases in energy and financial costs, leading to a reduction in the plant's overall efficiency. Bailera et al. [13] researched a Power to Gas-Oxycombustion system, incorporating methanation to boost efficiency and the use of CO_2. They discovered that this integrated approach elevates the system's overall efficiency from 55.9% to 67.5%. This method significantly enhances energy storage potential and diminishes environmental footprint by efficiently utilizing CO_2 and hydrogen.

Ashour et al. [14] introduced a study on the steady-state analysis of the Tripoli West low temperature horizontal tube multi-effect distillation (LT-HT-MED) plant, which was implemented to replace old multi-stage flash (MSF) units for boiler makeup water supply. The newly commissioned units mark the first operation of LT-HT-MED units, designed by Sidem, featuring a thermo-compressor that utilizes vapor produced in the last effect and live steam from the boiler. Khanmohammadi et al. [15] explored an integrated cogeneration system combining a Gas Turbine Cycle, MED with Thermal Vapor Compression, and an ORC. This system efficiently uses the waste heat from gas turbine exhaust to produce 39.6 MW of power and 137.3 kg/s of freshwater, achieving significant enhancements in energy and exergy efficiencies and a gain output ratio of 4.41. The study pinpointed major exergy losses primarily in the combustion chamber and MED unit, and highlighted the importance of optimizing operational parameters to improve overall system performance.

This paper investigates a system designed to generate energy, methane (CH4), and fresh water (distilled) by leveraging the heat from a Gas Turbine (GT) cycle, combined with a digester, Proton Exchange Membrane (PEM), and Multi-Effect Distillation (MED) processes. For a clearer understanding and justification of this concept, examining studies that utilize waste heat from gas turbines to produce methane and distilled water is beneficial. Such comparisons can elucidate the advantages and functionality of the proposed system. Montazerinejad et al. [16] explored an integrated system that merges a Proton Exchange Membrane (PEM) fuel cell with an organic Rankine cycle for the production of electricity. The study's conclusion highlights that the PEM fuel cell achieves an exergy efficiency of 46.89%, with the overall electrical efficiencies reaching 39.06% for the fuel cell alone and 44.81% for the system as a whole. A significant finding is the conventional exergy destruction rate for the combined system, measured at 484.4 kW, with the majority of this loss occurring within the PEMFC stack. Mofrad et al. [17] assessed an innovative geothermal-driven cogeneration system in Ardabil, Iran, aimed at producing power and hydrogen concurrently. This system capitalizes on geothermal energy extracted from hot water within Earth's crust layers, using steam turbines for power generation and the remaining heat to support a secondary cycle. With the use of a pentane-butane mixture, the system reports an energy efficiency of 19.34% and an exergy efficiency of 58.6%. Notable outcomes include the identification of a steam turbine experiencing high irreversibility, marked by an exergy destruction rate of 16.4 kW, and the determination of the lowest destruction cost for the employed working fluid at 23.3 USD per

hour. Additionally, the PEM electrolyzer, essential for hydrogen generation, was found to have a considerable environmental footprint, amounting to 259 mpts/h. Shamsi et al. [18] introduced a cutting-edge cogeneration system designed for the efficient production of green syngas and electricity, integrating a Proton Exchange Membrane electrolyzer with the Allam cycle. This system comprises a water electrolysis unit, the Allam power cycle, a water/ammonia power cycle, and an Organic Rankine Cycle. Their findings underscore the system's notable energy and exergy efficiencies, which stand at 60.44% and 63.22% respectively, alongside a substantial total exergy destruction rate of 10.97 MJ/kg of syngas produced. The Allam power cycle emerged as the major source of exergy destruction, contributing to 66% of the total. Assareh et al. [19] investigated a cogeneration module that merges compressed-air energy storage with electrolysis, utilizing methane and hydrogen. The research pinpointed methane as the most advantageous in terms of cost and CO_2 emissions reduction, showcasing a total cost rate of 68.073 USD/hour. The study also reported exergy destruction rates of 1706.38 kWh for the charging unit and 3019.31 kWh for the discharging unit. Moreover, this study highlights the system's superiority in energy round-trip efficiency, marking it as the most efficient approach evaluated. Behzadi et al. [20] introduced a novel cogeneration system integrating concentrated solar power with a vanadium chlorine cycle for enhanced hydrogen production. This innovative multi-generation plant, designed to support the global green-transition process, incorporates a central receiver-based concentrated solar system for high-temperature heat production, a vanadium chlorine thermochemical cycle for hydrogen generation using solar heat instead of natural gas, a thermoelectric generator (TEG) for additional power generation from excess heat, and a multi-effect desalination (MED) unit for water production from low-temperature waste heat. Among various optimization strategies, the multi-objective grey wolf algorithm emerged as the most effective, achieving 2.5% higher exergy efficiency, 1 $/GJ lower energy cost, and 0.12 kg/kWh reduced levelized CO_2 emissions compared to the baseline operation.

The main innovations and novel aspects are as follows:

- Optimization using the Gray Wolf Algorithm: This study applies the Gray Wolf Optimization algorithm to assess and optimize the performance conditions of Power-to-X systems, enhancing their efficiency and sustainability in fuel transportation.
- Integrated Approach for Renewable Methane Production: This research pioneers a novel system design that integrates solar-powered hydrogen production with carbon-neutral plants for methane production. This process utilizes excess CO_2 and involves a methanation unit, setting a precedent in the field.
- Waste Heat Utilization for Water Distillation: Another innovation introduced by this study is the use of waste heat from the Power-to-X system processes to power a Multi-Effect Distillation (MED) unit, thereby producing distilled water and further optimizing environmental benefits.

Nomenclature

A	Area [m^2]
BPE	Boiling point elevation
C_p	Unit cost of products [$/GJ]
$\dot{C}$	Cost rate [$/h]
CETD	Cold end temperature differer
CI	Cost index
CRF	Capital recovery factor
CV	Control volume
EES	Engineering equation solver
$\dot{E}x_D$	Exergy destruction rate [kW]
F	Faraday constant
g_i	Gibbs free energy of compone [J/mol]
G_i	Gibbs free energy of reaction i [J/mol]
GTC	Gas turbine cycle
GTIT	Gas turbine inlet temperature [K]
HRSG	Heat recovery steam generato
i_r	Interest rate
J	Current density [A/m^2]
Kpi	Equilibrium constant of reacti
L	Thickness of the membrane [μm]
LHV	Lower heating value [MJ/kg]

MED	Multi Effect Desalination
MOGWO	Multi − Objective grey wolf Optimiz
n	Plant lifetime [years]
N	Yearly operational duration [hours]
PEM	Proton Exchange Membrane
PVT	Photovoltaic thermal collector
SPECO	Specific Exergy Cost
U	Heat transfer coefficient
x	Molar fraction
$\dot{Z}$	Investment cost rate [$/h]
Greek symbo	
η_{en}	Efficiency of energy [%]
η_{ex} or η_{II}	Efficiency of exergy [%]
ε	Effectiveness factor [%]
σ	Local ionic conductivity
μ_i	Mole production of product [Kmol]
ϕ	Maintenance factor
ζ_{co_2}	Emission index [kg/kWh]
Subscripts	
0	Reference condition
CC	Combustion chamber
Cond	Condenser
Comp	Compressor
en	Energy
ex	Exergy
Eva	Evaporator
EV	Expansion Valve
GT	Gas turbine
HEX	Heat exchanger
in	Inlet
net	Net
out	Outlet
ph	Physical
Pu	Pump

2. Description of the proposed system

Figure 1 depicts an intricate system that amalgamates several advanced methods for energy generation and waste management, incorporating a gas turbine (GT), an organic Rankine cycle (ORC), a proton exchange membrane (PEM) electrolyzer, a methanation segment, and a multi-effect distillation (MED) unit. The GT, coupled with digesters, adeptly processes municipal solid waste to extract energy, while the ORC system converts surplus heat into electrical power. The PEM electrolyzer harnesses solar power to produce hydrogen, which is either stored or funneled into the methanation stage for methane synthesis. Additionally, the MED unit utilizes the thermal energy from the GT for seawater desalination, further improving energy efficiency and contributing to a sustainable output. This comprehensive framework is designed to enhance energy recovery, minimize waste, and promote environmental sustainability through the integration of various renewable and waste-to-energy technologies.

In Fig. 1, the process begins as air enters the GT cycle's compressor 1 (Comp 1) at (state 1) and is then compressed to (state 2). This compressed air is introduced into the combustion chamber (CC), reacting with biogas at (state 3) to produce a high-temperature flow at (state 4)—the biogas itself is derived from municipal solid waste via a digester. The resulting high-energy stream powers turbine 1 (Turb 1), generating electricity and exiting as waste heat at (state 5). This waste heat from state 5 preheats the fluid (stream 8), which subsequently powers the ORC's Turbine 2 (Tur2) at (state 9), creating additional electricity as the fluid expands and cools to (state 10). Exiting Turbine 2 at state 10, the working fluid enters the regenerator (Reg), cooling by transferring heat to the fluid from state 6, which is being preheated to (state 7). After cooling in the regenerator (state 11), the fluid progresses to the condenser. Post-condensation at state 6, the fluid is pressurized by Pump 1, moving it to (state 7). This pressurized fluid is reheated in the regenerator, absorbing heat and advancing to (state 8), where it receives further heat from the GT's exhaust gases, transferring from state 5 to 36. This sequence maximizes the use of the GT's waste heat to boost the overall thermal efficiency of the power plant.

Subsequently, the GT's exhaust gases at (state 36), having contributed to the heating stages, are channeled to the CO_2 Capture system, isolating carbon dioxide to reach (state 37). Here, a predominantly CO_2 gas stream is obtained, separating it from other exhaust components. Non-captured gases progress to (state 38) and are then vented through the stack (state 39), mitigating CO_2 emissions and enhancing the plant's environmental impact.

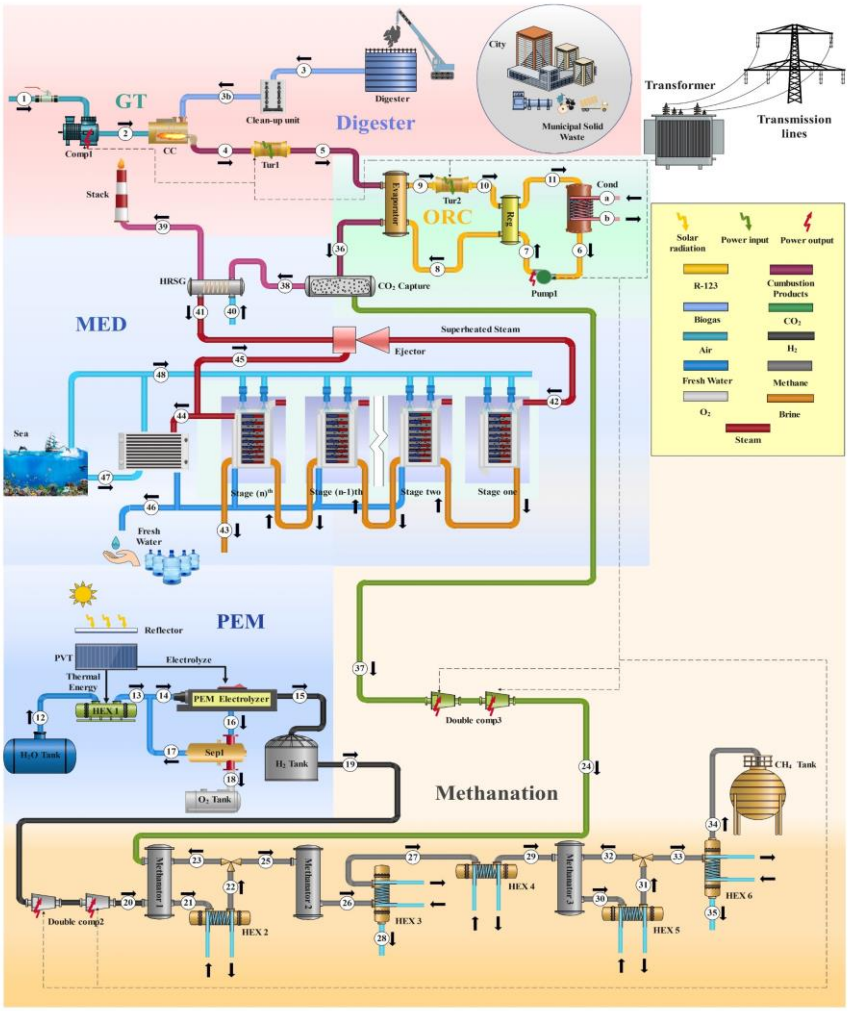

Fig. 1. Schematic representation of the planned cogeneration system designed to generate energy, as well as produce methane and distilled water.

In the methanation section, modeled after Bailera et al. [13], hydrogen generated from electrolysis (state 19) and CO_2 from (state 37) are compressed to 25 bar in multi-stage compressors (state 24), raising their temperature to obviate the need for additional heating before entering the first methanator (Meth 1). The gas exiting at (state 21) is cooled to 300°C at (state 22), and a large part of the flow from (state 23) is recirculated to manage the temperature within the system. After the second methanator (Meth 2) at (state 26), most of the water, which inhibits the methanation reaction, is condensed and removed at (state 28). The gas mixture then undergoes reheating to 300°C (state 29) before entering the third methanator (Meth 3). A recirculation loop after the third reactor manages 78% of the outlet flow at (state 32). The final water content is condensed at (state 35), resulting in dry synthetic gas ready for distribution into the gas network (CH_4 Tank) at (state 34). The methanation process is indeed complex and requires careful temperature management to prevent catalyst degradation. Our system implements a sophisticated control strategy that includes multi-stage compression with intercooling and staged methanation reactors with intermediate cooling to maintain optimal catalyst temperatures. Additionally, the reactors are designed to operate at a temperature below the threshold for catalyst sintering, and we utilize robust catalysts specifically developed for these conditions.

In the MED unit, modeled after Behzadi et al. [20], the evaporator outlet gases (state 39) are harnessed in the HRSG, where the water (state 40) absorbs heat to become steam. This steam enters the ejector (state 41) with high enthalpy and mixes with the secondary vapor (state 45) from the MED's last stage. The result of this

mixture is superheated steam (state 42), which then serves as the heat source for the first stage of desalination. Meanwhile, inlet seawater (state 47) flows into the condenser to condense the desalinated vapor (state 44), which originated from the final stage of the MED process. The condensed vapor at this point becomes distilled water (state 46), which is the output of the MED unit. The preheated seawater, after losing some of its heat to the process, is split with part used as feedwater across the stages and the remainder (state 48) returned to the sea. The brine, which is the more concentrated saltwater left after the evaporation (state 43), is moved to subsequent stages to continue the cycle of evaporation and condensation, enhancing system efficiency and vapor production for more distilled water.

Furthermore, a comprehensive depiction of the process flow diagram for addressing the issue statement presented in Fig. 1 may be shown in Fig. 2.

3. Mathematical modeling

In this paper, the Engineering Equation Solver (EES) was utilized to create a simulation, while MATLAB was employed for additional optimization to conduct the study discussed. This simulation integrates comprehensive evaluations of mass, energy, exergy, economics, and environmental impacts within the framework of thermodynamic principles.

This section also describes a multi-objective optimization strategy. Appendix A, Table A.1, and the subsequent section provide detailed elaboration on the primary assumptions supporting the models used in this research:

- Exergy loss due to carbon dioxide capture processes is regarded as minimal [21].
- At the compressor's inlet, air's molar composition consists of 79% nitrogen (N_2) and 21% oxygen (O_2) [21].
- Ambient conditions are present when cooling water is introduced into the condenser [22].
- Changes in both kinetic and potential energy are minimal and thus ignored [23].
- The network of piping incorporates considerations for pressure reductions [24].
- In each effect, the vapor generated undergoes complete desalination [25].
- The salinity of saltwater is 36%, whereas the highest salinity of brine is 70% [25].
- All effects exhibit identical temperature disparities [26].

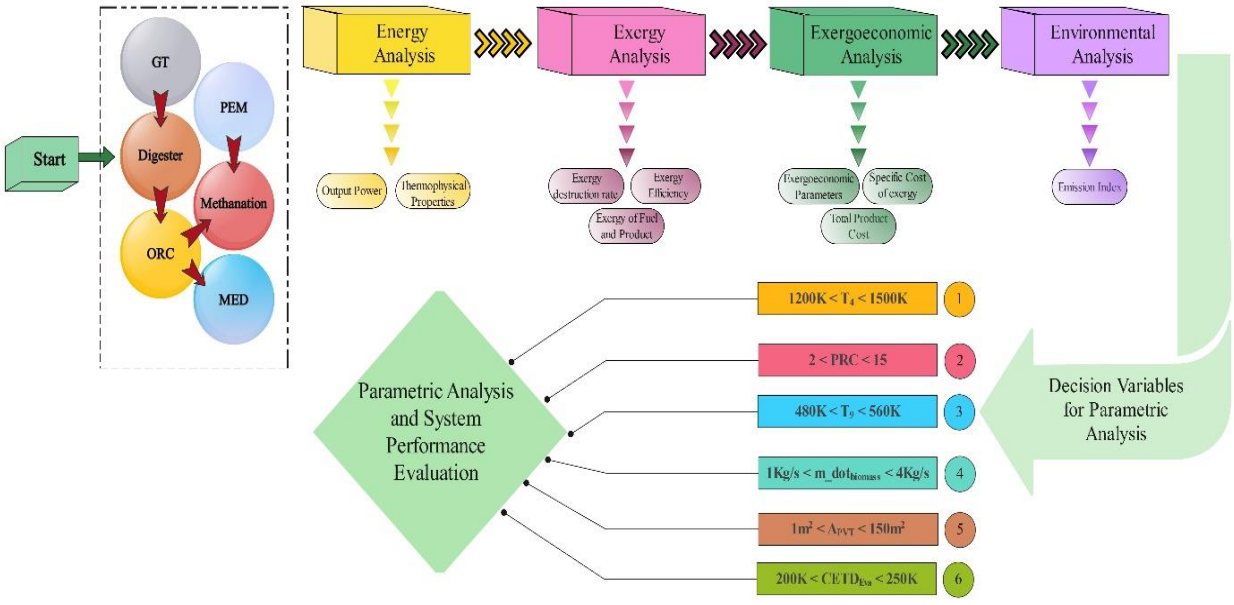

Fig. 2. Diagram illustrating the various stages of simulation in this study.

3.1. Energy and mass

The concept of energy preservation, based on thermodynamic principles, is applied to ascertain the state of each flow at the entry and exit points of the control volume, as illustrated by the mass and energy balance equations [27]:

$$\sum_{in}\dot{m}=\sum_{out}\dot{m} \tag{1}$$

$$\dot{Q}+\sum_{in}\dot{m}h=\sum_{out}\dot{m}h+\dot{W} \tag{2}$$

To maintain microbial activity, a thermophilic anaerobic digester operating at 328 °K was used for the digestion process. The biogas composition was determined using the organic (ash-free) portion of Municipal Solid Waste, following the method described by Zhang et al. [7]. The widely accepted reaction for biomass digestion is as follows:

$$C_nH_aO_b+wH_2O\rightarrow n_1CO_2+n_2CH_4 \tag{3}$$

3.2. MED unit

Compared to competing technologies, the MED system uses less energy and produces less heat, making it an attractive and economical option for producing drinkable water. Each subsystem's mass, salinity, and energy balance equations were solved in order to achieve the MED unit modeling. To calculate the temperature difference between effects, we can define T_{b1} and T_{bN} as the brine temperature at the 1st and Nth effects, respectively [28]:

$$\Delta T=\frac{T_{b1}-T_{bN}}{N-1} \tag{4}$$

In addition, the temperatures of the brine and water vapor are evaluated at the subsequent effect by [28]:

$$T_{bi+1}=T_{bi}-\Delta T \tag{5}$$

$$T_{vi}=T_{bi}-BPE \tag{6}$$

In this context, BPE refers to the increase in boiling point. The cooldown temperature of brine, denoted as T_i', is calculated as the total of the non-equilibrium allowance (NEA_i) and the brine temperature (T_{bi}) [29]:

$$T_i^{'}=T_{bi}+NEA_i \tag{7}$$

The steam ejector's energy balances are expressed as follows:

$$M_mh_m+D_rh_g=\left(M_m+D_r\right)h_s \tag{8}$$

Table 1 lists the thermodynamic equations for the condenser and each effect of the MED unit.

For the first and subsequent effects up to the N^{th} effect, as well as for the condenser, the necessary areas of heat transfer for the successful implementation of the Multi-Effect Distillation model are described by [30]:

$$A_1=\frac{M_sL_s}{U_{e1}\left(T_S-T_1\right)} \tag{9}$$

$$A_i=\frac{\left(D_{i-1}+D_{i-1}'\right)L_{i-1}}{U_{ei}\Delta T_i} \tag{10}$$

$$A_C=\frac{\left(D_N+D_N'-D_r\right)L_W}{U_cLMTD_C} \tag{11}$$

Table 1. Energy and mass balance calculations for all MED unit effects [28].

1st effect	Mass balance	$B_1=F_1-D_1$
	Salinity balance	$X_1=\frac{F_1}{B_1}X_f$
	Energy balance	$M_mL_m=D_1L_1+F_1C_P(T_1-T_F)$
2 to N effect	Mass balance	$B_i=B_{i-1}+F_i-D_i$
	Salinity balance	$X_i=\frac{F_i}{B_i}X_f+\frac{B_{i-1}}{B_i}X_{i-1}$
	Energy balance	$(D_{i-1}+D'_{i-1})L_{i-1}=D_iL_i+F_iC_P(T_i-T_F)+B_iC_P(T_i-T_{i-1})$

Here, U_e stands for the total i[th] effect heat transfer coefficient and U_c for the condenser heat transfer coefficient; the formulas for both coefficients are [30]:

$$U_e = 1,9394 + 1,40562\times10^{-3}\times T_b - 2,07525\times10^{-5}\times T_b^{\,2} + 2,3186\times10^{-6}\times T_b^{\,3} \quad (12)$$

$$U_c = 1,7194 + 3,2063\times10^{-3}\times T_V + 1,5971\times10^{-5}\times T_V^{\,2} + 1,9918\times10^{-7}\times T_V^{\,3} \quad (13)$$

3.3. Methanation unit

In reactors, the conversion of CO_2 into methane can be divided into two separate steps. The first step involves the reverse water-gas shift reaction, as depicted in Eq (15). This is followed by the methanation of CO, as described in Eq (16) [31].

$$CO_2 + 4H_2 \leftrightarrow CH_4 + 2H_2O \qquad \Delta H_{298\,K} = -165\,KJ/mol \quad (14)$$

$$CO_2 + H_2 \leftrightarrow CO + H_2O \qquad \Delta H_{298\,K} = +41,2\,KJ/mol \quad (15)$$

$$CO + 3H_2 \leftrightarrow CH_4 + H_2O \qquad \Delta H_{298\,K} = -206,1\,KJ/mol \quad (16)$$

The stoichiometric coefficients, expressed in kilomoles, are utilized to determine the products of CO_2 methanation by applying the mole balance to the overall reaction:

$$v_{CO_2}CO_2 + v_{H_2}H_2 + v_{CH_4}CH_4 + v_{H_2O}H_2O + v_{CO}CO \leftrightarrow \mu_{CO_2}CO_2 + \mu_{H_2}H_2 + \mu_{CH_4}CH_4 + \mu_{H_2O}H_2O + \mu_{CO}CO \quad (17)$$

In this particular framework, the variable v_i denotes the initial mole quantity of each reactant, whereas μ_i pertains to the mole quantity of each product subsequent to the reaction. The determination of the composition of the gas post-reaction relies heavily on the values of the five key unknowns, which represent the products. In order to determine these values, it is necessary to take into account the mole balances for carbon, hydrogen, and oxygen, as specified in Eq. (18 to 20), in addition to the equilibrium constants for the reactions, which are provided in Eq. (21 and 22):

Carbon balance:

$$v_{CO_2} + v_{CH_4} + v_{CO} = \mu_{CO_2} + \mu_{CH_4} + \mu_{CO} \quad (18)$$

Hydrogen balance:

$$v_{H_2} + 2v_{CH_4} + v_{H_2O} = \mu_{H_2} + 2\mu_{CH_4} + \mu_{H_2O} \quad (19)$$

Oxygen balance:

$$v_{CO_2} + \frac{1}{2}v_{H_2O} + \frac{1}{2}v_{CO} = \mu_{CO_2} + \frac{1}{2}\mu_{H_2O} + \frac{1}{2}\mu_{CO} \quad (20)$$

Reverse water – gas shift:

$$Kp_{RWGS} = \frac{x_{CO}.x_{H_2O}}{x_{CO_2}.x_{H_2}} = \frac{\mu_{CO}.\mu_{H_2O}}{\mu_{CO_2}.\mu_{H_2}} \quad (21)$$

CO methanation:

$$Kp_{CO} = \frac{x_{CH_4}.x_{H_2O}}{x_{CO}.x_{H_2}^3}.\left(\frac{P_r}{P_a}\right)^{-2} = \frac{\mu_{CH_4}.\mu_{H_2O}.\left(\mu_{CO_2}+\mu_{H_2}+\mu_{CH_4}+\mu_{H_2O}+\mu_{CO}\right)^2}{\mu_{CO}.\mu_{H_2}}.\left(\frac{P_r}{P_a}\right)^{-2} \quad (22)$$

The symbol Kp_i represents the equilibrium constant of the i-th reaction. The variable x_i denotes the mole-based proportion of each component i, determined under wet conditions. The variable P_r represents the internal pressure within the reactor, whereas P_a denotes the pressure exerted by the nearby environment. The determination of the value of Kp_i is explicitly derived from the formula presented in Eq. (23) [32].

$$Kp_i = e^{-\frac{G_i}{\bar{R}T_r}} \quad (23)$$

G_i represents the Gibbs free energy associated with reaction i, as explained in Eq. (24 and 25). The term T_r denotes the temperature inside the reactor. Significantly, the Gibbs free energy for each component is determined using the formula $g = h - T_r s$, as explained in Eq. (24 and 25):

$$G_{RWGS} = g_{H_2O} + g_{CO} - g_{H_2} - g_{CO_2} \quad (24)$$

$$G_{CO} = g_{CH_4} + g_{H_2O} - 3g_{H_2} - g_{CO} \quad (25)$$

In conclusion, the determination of the temperature within the reactor is achieved by employing an energy balance, as described in Eq. (26). The enthalpies of the reactions specified in Eq. (15) and (16) are included in this calculation. One crucial simplification in this methodology is the underlying assumption that the entirety of the exothermic heat released is solely utilized to elevate the temperature of the reaction products from their initial state to their ultimate state:

$$\sum_i Cp_i.\mu_i.\left(T_r - T_{in}\right) = -.H_{RWGS}.\left(v_{CO_2} - \mu_{CO_2}\right) \\ -.H_{CO}.\left(v_{CO_2} - \mu_{CO_2} - \mu_{CO}\right) \quad (26)$$

3.4. Exergy analysis

Exergy is the ultimate work potential that can be extracted from a system in combination with its environment as they achieve a state of equilibrium. This analysis serves as a potent means to pinpoint the locations, nature, and magnitude of inefficiencies present in a system, assessing their potential for recovery or inevitable loss [33].

In scenarios where the system's movement relative to its surroundings is nil (thus, kinetic and potential exergies are nullified), exergy is divided into two main types: physical and chemical. Physical exergy is the peak work potential during the system's transition from its starting condition, defined by the equation [34]:

$$e^{PH} = \left(h - h_0\right) - T_0\left(s - s_0\right) \quad (27)$$

where e^{PH} is the physical exergy, with h and s denote the specific enthalpy and entropy relative to reference conditions (h_0 and s_0) based on standard temperature T_0 and pressure P_0. The derivation of molar chemical exergy for a perfect mix is presented as [35]:

$$e^{CH} = \sum x_i e_i^{CH} + \bar{R}T_0 \sum x_i \ln x_i \quad (28)$$

In the formula, x_i indicates each component's molar fraction and its base chemical exergy e_i^{CH}, with $\bar{R}$ signifying the universal gas constant.

3.5. Exergoecomic analysis

Specific exergy costing (SPECO) is a method used within the field of thermoeconomics or exergoeconomics, which combines principles from thermodynamics, particularly exergy analysis, with economic analysis. By integrating the concept of exergy with financial analysis and utilizing a cost balance equation, the SPECO method facilitates a comprehensive synthesis for this evaluation [36]:

$$\dot{C}_q + \sum \dot{C}_{in} + \dot{Z} = \dot{C}_w + \sum \dot{C}_{out} \quad (29)$$

Where, $\dot{C}_q$ is the heat loss cost rate, capturing the cost associated with energy losses in the system. The term $\sum \dot{C}_{in}$ denotes the cumulative cost rate of all inputs, including raw materials and energy inputs. $\dot{Z}$ represents the investment cost rate, reflecting the capital expenses incurred for the system. On the other side of the equation, $\dot{C}_w$ stands for the cost rate of the work produced by the system, and $\sum \dot{C}_{out}$ corresponds to the total cost rate associated with the system's outputs, encompassing both the valuable products and byproducts.

Concerning the unit cost of exergy (c), the subsequent Eq. (30 – 33) is utilized to calculate the terms mentioned above [36]:

$$\dot{C}_q = c_q \dot{Q}_j \left(1 - \left(\frac{T_0}{T_j}\right)\right) \quad (30)$$

$$\dot{C}_w = c_w \dot{W}_{cw} \quad (31)$$

$$\dot{C}_{in} = c_{in} \dot{E}_{in} \quad (32)$$

$$\dot{C}_{out} = c_{out} \dot{E}_{out} \quad (33)$$

$$\dot{Z} = Z \times \left(CRF\, \varphi / N\right) \quad (34)$$

In the Eq. (34), CRF, φ, and N each denote the capital recovery factor, the maintenance factor, and the system's yearly operational duration, respectively. The calculation of the CRF involves considering the cycle's lifespan (n) and the applicable interest rate (i_r), as indicated by the subsequent equation [36]:

$$CRF = \frac{\left(i_r \left(1 + i_r\right)^n\right)}{\left(\left(1 + i_r\right)^n - 1\right)} \quad (35)$$

Equation (35) can be revised to incorporate the adjusted rate of investment cost. Therefore, the equation is updated with the following relation [36]:

$$\dot{Z}_{PY} = \dot{Z}_{ref} \times \left(CI_{PY} / CI_{ref}\right) \quad (36)$$

This formula demonstrates that by factoring in the chemical index (CI) of the plant for both the reference and current years, the rate of investment cost from the reference year can be adjusted to reflect the values for the current year (PY).

3.6. Environmental analysis

The examination of energy systems has consistently incorporated the adverse effects of plants on the environment as a significant determinant. The utilization of renewable energy sources in lieu of fossil fuels is a widely

recognized approach within this domain. Contrary to popular belief, renewable energy technologies have been found to have adverse effects on the environment. The evaluation of such consequences can be conducted through the utilization of exergo-environmental approaches that are grounded in exergy-based principles. Enhancing the efficacy of second-law processes through design can be achieved by minimizing the overall exergy destruction of the plant, as quantified by the exergy concept. This leads to reduced resource consumption for an equivalent quantity of electricity. The environmental ramifications of escalating fuel consumption will undoubtedly be more significant. In the following section, three exergo-environmental indicators are presented, which are contingent upon the reference [37]:

$$\varepsilon_{ei} = \frac{\dot{E}_{D,tot}}{\dot{E}_{Input}} \tag{37}$$

$$\varepsilon_{ed} = \frac{\varepsilon_{ei}}{\eta_{II}} \tag{38}$$

$$\varepsilon_{es} = \frac{\dot{E}_{D,tot}}{\dot{E}_{D,tot} + \dot{E}_{Product} + 1} \tag{39}$$

3.7. Multi-objective optimization

Given the dynamic nature of energy demand, fuel prices, and regulatory environments, adaptability and forward planning are crucial in the energy industry. Optimization models, with their ability to enhance system flexibility and consider multiple scenarios, offer significant advantages. They pave the way for improved management of demand response programs,
integration of renewable energy sources, and optimization of energy storage systems. Neural Net Fitting is utilized to create a surrogate model of the system's performance, which accurately predicts outputs for a wide range of inputs based on historical data. This approach significantly reduces the computational load during optimization, as it eliminates the need for time-consuming simulations for each iteration. The neural network model serves as an efficient, accurate approximation for the system's behavior, streamlining the Grey Wolf optimization process. In summary, optimization should be a top priority for energy systems aiming to reduce costs, carbon emissions, and resource consumption. Optimization techniques empower energy sector planners to design and manage systems that are more cost-effective, environmentally friendly, flexible, and efficient. The optimization process is depicted in the flow diagram in Fig. 3.

4. Validation

The purpose of this part is to verify the correctness of the simulations conducted in previous sections in order to provide a rationale for the acquired findings. The present work aims to evaluate the PEM unit, Methanation system, and MED unit models via a comparative analysis with the models documented in the existing literature review. The study done by Ni et al. [10] and Ioroi et al. [38] provides clarification on the validity of the PEM modeling. Figure 4 illustrates the relationship between cell potential and current density. According to Fig. 4, the absolute average difference between the present study and the research conducted by Ioroi et al. [38] is less than 0.35%.

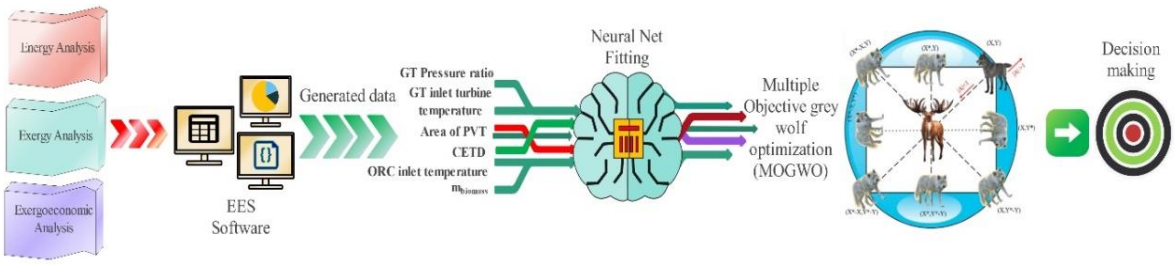

Fig. 3. Methodology for thorough modeling and optimization.

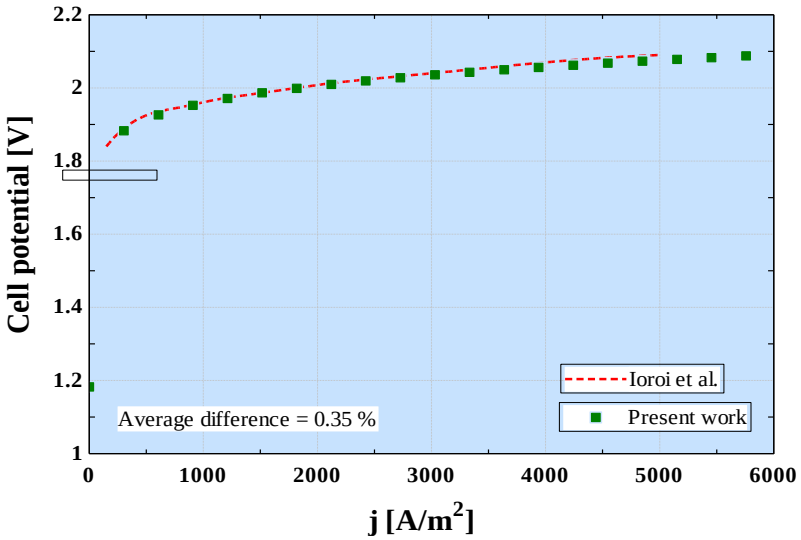

Fig. 4. Evaluate the proton exchange membrane unit by comparing it to the results informed by Ioroi et al. [38].

In addition, our model predicted the temperature and mass flow rates at different state points, together with the pressure values for the methanation unit, as shown in Table 1. After doing a comparative analysis with the reference data, it was determined that the largest disparity between the outcomes derived from our model and the reference was a measly 2.96%. The little difference highlights the exceptional level of precision and dependability in the forecasts generated by our model, thereby affirming its appropriateness for representing the methanation unit in the proposed system.

The final, the effectiveness of the MED unit is verified by comparing it to the data from an actual plant, which is shown in Table 2. The current model has a high level of accuracy, as seen by the consistent outcomes obtained when design parameters are held constant.

Table 2. Evaluate the methanation unit by comparing it to the results informed by Bailera et al.[39].

State No.	Pressure (bar)	Present work temperature (°C)	Ref [40] temperature (°C)	Error Percentage (%)	Present work mass flow rate (kg/s)	Ref [40] mass flow rate (kg/s)	Error Percentage (%)
14	25.0	308.6	308.6	0.00	7.04	7.20	-2.22
17	25.0	333.2	333.2	0.00	1.29	1.30	-0.76
18	25.0	596.7	591.6	0.86	37.87	38.50	-1.63
19	25.0	300	300.0	0.00	37.87	38.50	-1.63
20	25.0	300	300.0	0.00	30.10	29.54	1.89
21	25.0	300	300.0	0.00	8.33	8.50	-2.00
22	25.0	463.6	460.5	0.67	8.33	8.50	-2.00
23	25.0	197.4	197.4	0.00	4.80	4.90	-2.04
24	25.0	197.4	197.4	0.00	3.53	3.50	0.85
25	25.0	300	300.0	0.00	3.53	3.50	0.85
26	25.0	352.6	354.4	-0.50	16.05	16.00	0.31
27	25.0	300	300.0	0.00	16.05	16.00	0.31
28	25.0	300	300.0	0.00	12.52	12.50	0.16
29	25.0	300	300.0	0.00	3.53	3.50	0.85
30	25.0	155.7	155.7	0.00	2.62	2.70	-2.96
31	25.0	155.7	155.7	0.00	0.91	0.90	1.11

5. Results

5.1. Parametric study

Figure 5 depicts a dual-axis schematic that establishes a relationship between the dimensions of a photovoltaic-thermal (PVT) system and the rates of methane production as well as the emission index. The x-axis of the PVT area can be adjusted within a range of 1 to 150 m2. The left y-axis, shown by the teal color, illustrates the rate of methane generation ($\dot{m}_{ch_4}$), which demonstrates a positive association with the increasing size of the PVT zone. Consequently, a larger PVT area enables a greater amount of hydrogen to be generated by an electrolyzer, which is subsequently converted into methane. The right y-axis displays the emission index (ζ_{co_2}) in purple, exhibiting a positive association with the PVT area. The provided context suggests that an increase in the emission index is associated with a corresponding decrease in the value of commodities. Consequently, while the PVT area does contribute to the creation of methane, it may also result in higher emissions per unit of energy output (Kg_{co_2}/KWh). The graph illustrates the relationship between the expansion of renewable energy production capacity and its impact on emissions. There was a 14486.09% increase in the rate of methane generation, accompanied by a 6843.95% rise in emissions. This results in a nearly 145-fold rise in methane production and an almost 69-fold increase in emissions. The technology fits into a decarbonization strategy by providing a renewable method to produce methane, which could replace fossil-fuel-derived natural gas. While there is an increase in emissions due to greater methane production, the PVT system creates a renewable and potentially carbon-neutral source of methane, assuming the CO2 utilized in methanation is captured from the atmosphere or from emission points. This would represent a closed carbon cycle with a neutral or even negative carbon footprint when all system aspects are considered.

The diagram shown in Fig. 6 depicts the correlation between the dimensions of a PVT system and two distinct metrics, namely exergetic efficiency and the cost per unit of output. The graph's horizontal axis represents the extent of the PVT system's coverage, spanning from 1 to 150 square meters. The pink line on the left y-axis represents the exergetic efficiency, expressed as a percentage. The data exhibits a declining pattern as the PVT region undergoes expansion. Therefore, when the size of the PVT system increases, there is a corresponding increase in the quantity of solar energy being provided, resulting in a bigger factor in the efficiency calculation.

As a result, this phenomenon results in a reduction in the total exergetic efficiency. The unit cost of the product in ($/GJ) is shown by the green line on the right y-axis. It has been observed that the cost of the PVT grows proportionally with the expansion of its area. This observation might be interpreted as an indication that larger PVT systems are associated with higher capital expenditures, thereby resulting in an increased cost per unit of energy generated. The graphical representation of the intersection between the two measurements effectively depicts the trade-off between efficiency and cost as the system's size fluctuates. The exergetic efficiency decreased by 15.13%, whereas the C_p increased by 26.26%.

Table 3. Evaluate the MED unit by comparing it to the results informed by Ashour [14]

Design conditions	Present work	Real plant [13]
Number of effects	6	6
Motive steam rate (kg/s)	21.20	21.20
The pressure of motive steam (bar)	25	25
Minimum temperature of brine (°C)	42.8	42.8
Top brine temperature (°C)	61.80	61.80
Seawater temperature (°C)	30	30
Performance indicators		
Desalinated water (kg/s)	188.24	184.4
Gain output ratio	8.78	8.6

area. The provided context suggests that an increase in the emission index is associated with a corresponding decrease in the value of commodities. Consequently, while the PVT area does contribute to the creation of methane, it may also result in higher emissions per unit of energy output (Kg_{co_2}/KWh). The graph illustrates the relationship between the expansion of renewable energy production capacity and its impact on emissions. There was a 14486.09% increase in the rate of methane generation, accompanied by a 6843.95% rise in emissions. This results in a nearly 145-fold rise in methane production and an almost 69-fold increase in emissions. The technology fits into a decarbonization strategy by providing a renewable method to produce methane, which could replace fossil-fuel-derived natural gas. While there is an increase in emissions due to greater methane production, the PVT system creates a renewable and potentially carbon-neutral source of methane, assuming the CO2 utilized in methanation is captured from the atmosphere or from emission points. This would represent a closed carbon cycle with a neutral or even negative carbon footprint when all system aspects are considered.

The diagram shown in Fig. 6 depicts the correlation between the dimensions of a PVT system and two distinct metrics, namely exergetic efficiency and the cost per unit of output. The graph's horizontal axis represents the extent of the PVT system's coverage, spanning from 1 to 150 square meters. The pink line on the left y-axis represents the exergetic efficiency, expressed as a percentage. The data exhibits a declining pattern as the PVT region undergoes expansion. Therefore, when the size of the PVT system increases, there is a corresponding increase in the quantity of solar energy being provided, resulting in a bigger factor in the efficiency calculation.

As a result, this phenomenon results in a reduction in the total exergetic efficiency. The unit cost of the product in ($/GJ) is shown by the green line on the right y-axis. It has been observed that the cost of the PVT grows proportionally with the expansion of its area. This observation might be interpreted as an indication that larger PVT systems are associated with higher capital expenditures, thereby resulting in an increased cost per unit of energy generated. The graphical representation of the intersection between the two measurements effectively depicts the trade-off between efficiency and cost as the system's size fluctuates. The exergetic efficiency decreased by 15.13%, whereas the C_p increased by 26.26%.

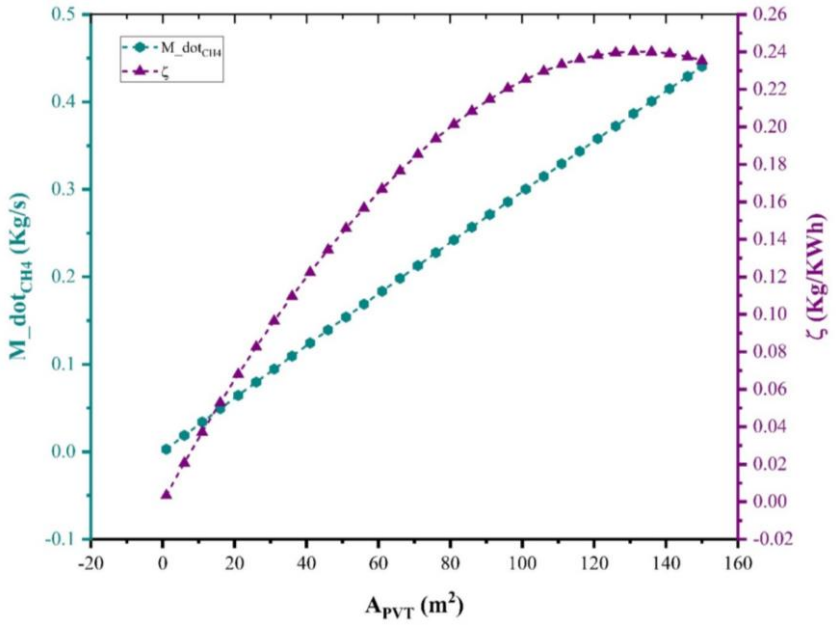

Fig. 5. The impact of the specific surface area of the PVT on the methane generation rate and emission index.

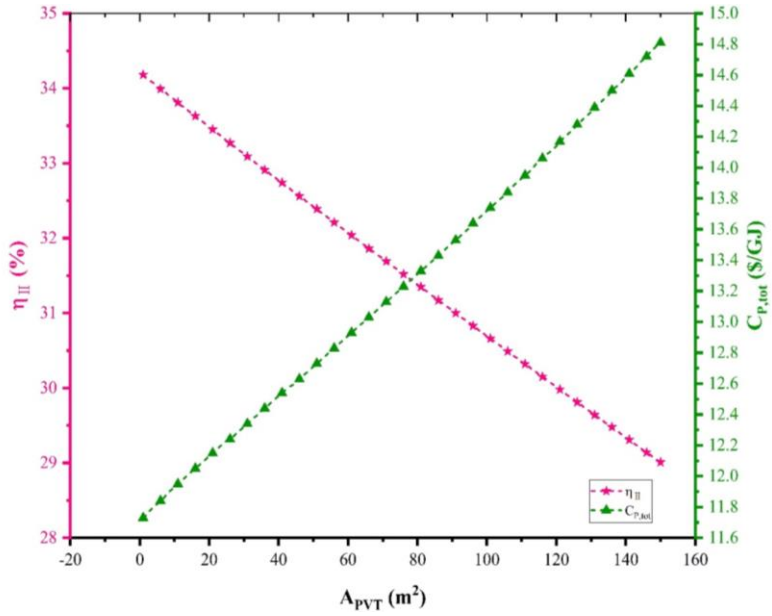

Fig. 6. The impact of the specific surface area of the PVT on the exergetic efficiency and unit cost of the product.

Moreover, Fig. 7 presents the impact of CETD in relation to ζ_{co_2} and D_{tot}. The declining pattern in the net power production leads to a 6.11% rise in the ζ_{co_2}. The orange scale represents the aggregate amount of distilled water D_{tot} generated during the process of cogeneration. As the CETD increases, the overall volume of distilled water first rises and then declines. The rise in outlet temperature of the water is attributed to the heat, which facilitates the production of a greater quantity of treated water. The maximal rate of desalination is 25.39 kg/s. The initial increase in distilled water production with rising CETD can be attributed to enhanced thermal energy available for the desalination process. However, beyond a certain temperature threshold, the efficiency of heat transfer may decrease, or thermal degradation of system components may occur, leading to a decline in water production. The exact cause of this decline is subject to further investigation, and it may be a combination of both thermal inefficiencies and the technical limitations of the current desalination technology employed in the cogeneration system.

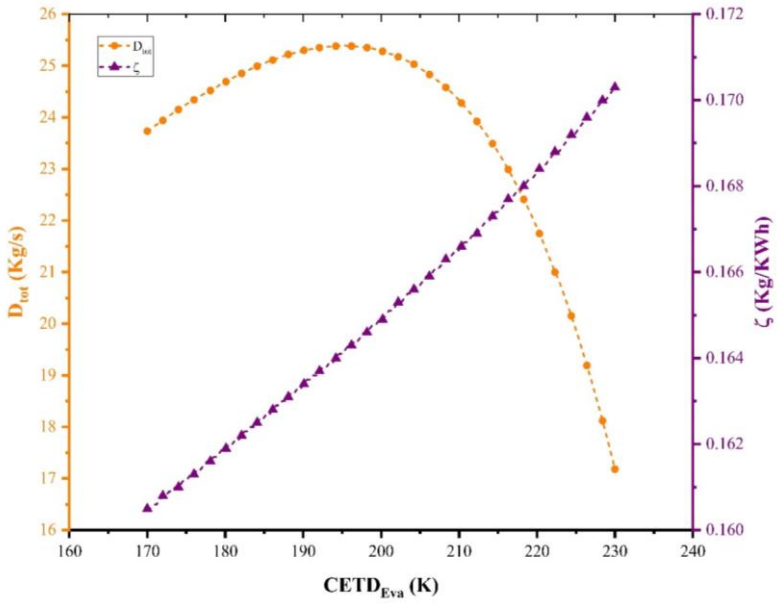

Fig. 7. The impact of CETD of the evaporator on emission index and total distilled water.

The performance indices of the whole system are significantly influenced by the pressure ratio, since the gas turbine is positioned upstream of the suggested designs. Fig. 8 displays the pressure ratio, ranging from 2 to 20 on the x-axis. The y-axis displays the exergetic efficiency and unit cost of items. The exergetic efficiency has a bell-shaped curve, first increasing with the pressure ratio, reaching its highest point, and thereafter decreasing. The reason for this is because until certain pressure ratio values are attained, the increase in compressor power is less significant compared to the rise in turbine power, resulting in an upward trend. The observed pattern indicates a favorable location for the pressure ratio, whereby the system exhibits optimal performance. If the pressure ratio exceeds a certain threshold, the performance of the system may deteriorate beyond this point due to a decrease in efficiency. The max value is 35.95%.

On the contrary, a 'U'-shaped curve emerges when the unit cost of items experiences a significant decrease as the pressure ratio increases, followed by a subsequent decrease and subsequent increase. This tendency also implies that in order to achieve cost-effective power production, there exists a favorable position for pressure ratios that effectively mitigate expenditures. At higher pressure ratios, the system's cost-effectiveness diminishes as expenditures increase beyond this threshold. The minimal value is 12.77 $\$/GJ$.

The carbon dioxide emissions (ζ_{co_2}) and total distilled water as a result of the pressure ratio are shown in the second graph (Fig. 9). However, as the pressure ratio increases, the value of ζ_{co_2} decreases significantly until it reaches a plateau, after which it stabilizes and decelerates. It is apparent that increasing the pressure ratio significantly improves the environmental performance of the system by reducing CO_2 emissions per unit of energy produced, up to a certain threshold. However, the benefits of decreasing emissions diminish if this threshold is reached. The lowest value recorded is 0.1512 kg/kWh. Moreover, the distilled water product as a whole demonstrates an increase as a consequence of the elevated pressure ratio of the gas turbine, leading to a higher rate of water flow to the MED unit. The flow rate has increased by 96.17%.

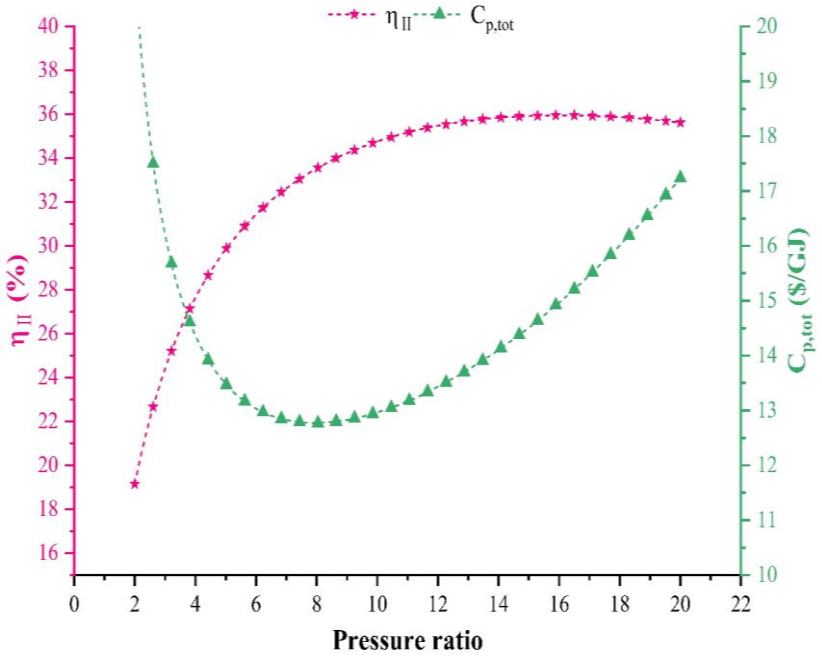

Fig. 8. The impact of the pressure ratio of GT on exergy efficiency and unit cost of products.

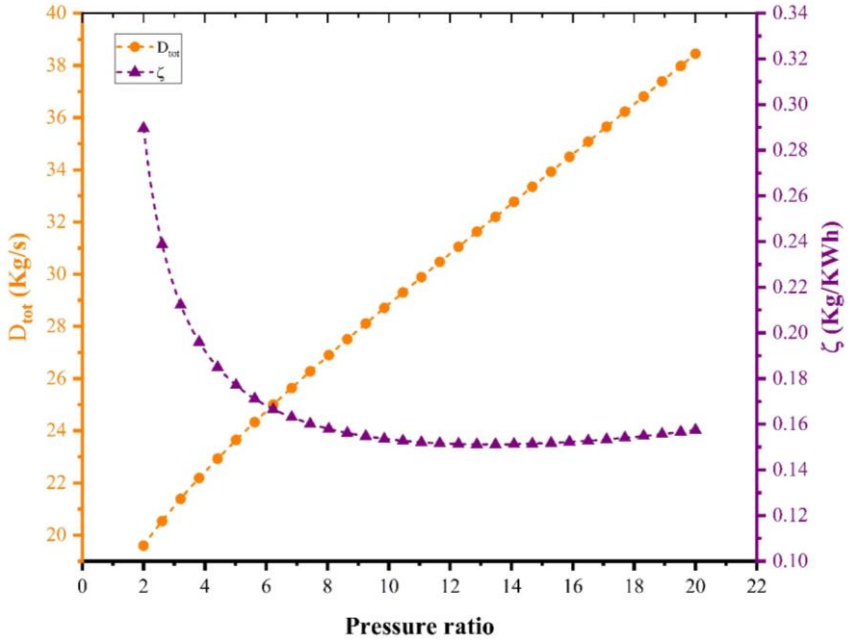

Fig. 9. The impact of the pressure ratio of GT on emission index and total distilled water.

The last criterion to be examined in this context is the GTIT, as seen in Fig. 10 and Fig. 11, correspondingly. The figures illustrate the impact of the turbine inlet temperature (TIT) on the performance of the system under two distinct conditions. The first graph displays T4, with a Kelvin value ranging from 1150 to 1550 K on the x-axis. The y-axis represents the exergetic efficiency and unit cost of the product. There was a 3.90% improvement in exergetic efficiency. The increased intake enthalpy of the GT turbine is the underlying cause for this phenomenon. The unit cost exhibits a reverse U-shaped pattern, whereby it first increases with temperature, reaches a low at around 1475 K, and thereafter experiences a further increase.

The following graph presents a comparison between ζ_{co_2} and total distilled water in relation to T_4. CO_2 emissions decrease in a linear manner as T_4 increases. This demonstrates that the amount of CO_2 emissions per unit of energy produced decreases as the temperatures at the turbine intake grow. The reason for this is because an increase in T_4 leads to a corresponding increase in net power production, resulting in a reduction in emissions by 9.95%. This phenomenon may be attributed to the enhanced efficiency of combustion and conversion processes at higher temperatures. These observed patterns indicate a complex interaction between emissions, efficiency, cost, and the temperature prevailing at the turbine intake. Several elements, such as system design, working fluid parameters, and operating conditions, have the potential to influence the optimal turbine intake temperature in order to maximize efficiency while minimizing costs and emissions. The objective of system designers and operators is to achieve a harmonious equilibrium between efficiency, cost, and environmental impacts. Under such circumstances, it is advisable for them to examine the graphs, which illustrate the existence of trade-offs that must be taken into account when selecting the operating temperature. Furthermore, the overall distilled water product exhibits a reduction due to the increased T_4 of the gas turbine, resulting in a decreased rate of water flow to the MED unit. The rate of flow has seen a reduction of 42.07%. In cogeneration systems, there is often a trade-off between maximizing power production and other utilities such as water production. An increase in T4 enhances the GT's power output, but it also reduces the waste heat available for the MED unit, leading to a decrease in water production. Therefore, when optimizing these systems, it's essential to find a balance that meets the desired energy output without compromising the need for water, especially in regions where water scarcity is an issue.

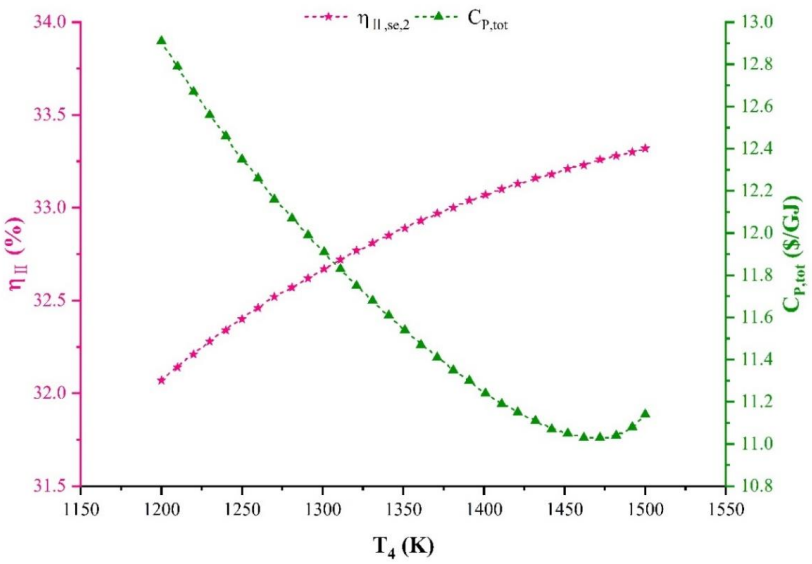

Fig. 10. The impact of GTIT (combustion temperature) on exergy efficiency and unit cost of products.

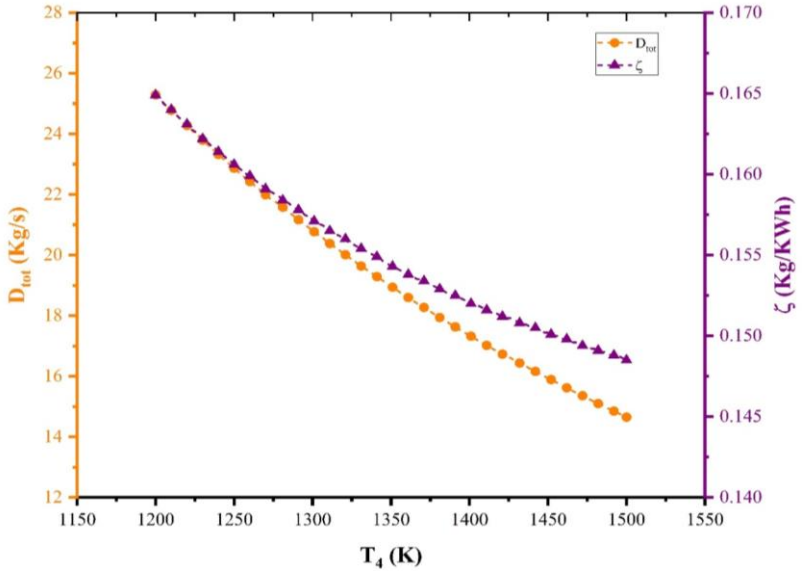

Fig. 11. The impact of GTIT (combustion temperature) on emission index and total distilled water.

In Fig. 12, we present here illustrates a clear trend: as the number of effects in a MED unit increases, so does the total production of distilled water. The graph, labeled with the variable D_{tot} to represent the total distilled water, displays a series of vertical bars, each corresponding to the number of effects ranging from 3 to 9. At the lower end, with three effects, the total distilled water production is measured at approximately 11.26 kg/s. There is a notable incremental rise with each additional effect. For instance, with four effects, the production climbs to around 16.08 kg/s. This positive correlation continues with impressive consistency, with the highest observed output reaching approximately 33.94 kg/s at nine effects. This data suggests that investment in technology to increase the number of effects within MED units could significantly enhance water production. These findings are essential for regions where water scarcity is a critical issue and could inform the design of future desalination infrastructure to maximize efficiency and sustainability. When considering increasing the number of effects in a MED unit for water-scarce regions, it's essential to consider the availability and cost of energy since MED units are energy-intensive. Other factors include capital and operational costs, environmental

regulations, potential scalability, and integration with existing water supply infrastructure. Long-term sustainability, especially the sourcing of energy from renewable resources, should also be a primary consideration to ensure the increased production aligns with environmental and economic goals.

5.2 Optimization results

The variables depicted in Fig. 13, namely the index factor, exergy efficiency, and unit exergy cost of the product, have been selected for the optimization scenario. The goal of this optimization is to find the best possible settings for the operation that will maximize exergy efficiency while minimizing the C_p and the ζ_{co_2} Index factor. The optimal exergy efficiency, unit product cost, and ζ_{co_2} Index factors are determined to be 37.53%, 8.402 $\$/GJ$, and 0.0134 kg/kWh, respectively, according to the optimization findings.

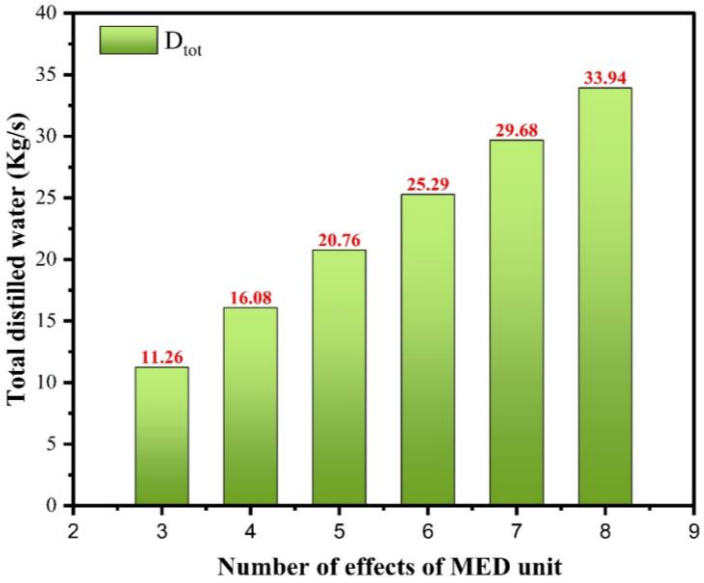

Fig. 12. The impact of number of effects of MED unit total distilled water.

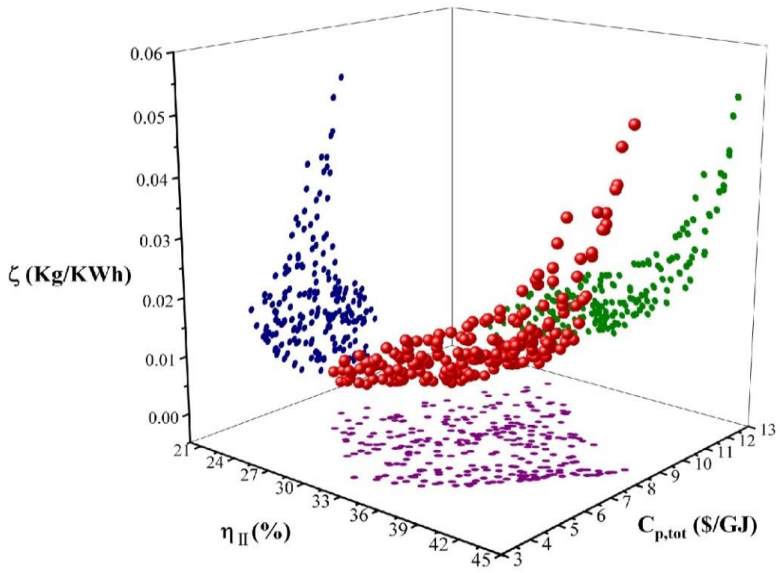

Fig. 13. Optimal solution for the first case of multi-objective optimization.

Additionally, following the analysis of the cogeneration system across the optimized scenario, the consolidated result is showcased in Table 3.

The graphical representation in Fig. 14 illustrates the dispersed distribution of data points obtained throughout the optimization process. The findings for various parameter combinations, such as the pressure ratio of GT, gas TIT, and biomass flow rate, are depicted in Fig. 14. Figure 14(a-c) displays that, as the population size increases, it becomes evident that there are patterns in the optimal values of specific parameters. Based on statistical data, it can be observed that as the population size expands, the optimal biomass flow rate value tends to tend to cluster around 1.25-2kg/s. Additionally, analysis indicates that the GT pressure ratio tends to cluster around 4-8. While increasing GTIT does enhance system performance by improving thermal efficiency, there is indeed a practical limit. This limit is determined by the temperature tolerance of the turbine materials, the cooling technology available, and the impact on the overall life cycle and maintenance costs of the system. In our optimization model, we included these as constraints to ensure the solutions remained within a realistic operational range.

Table 3. Enhanced performance metrics of the suggested framework.

Optimization first case		
η_{ex} (%)	$C_p(\$/GJ)$	ζ_{co_2} (kg/kWh)
37.53	8.402	0.0134

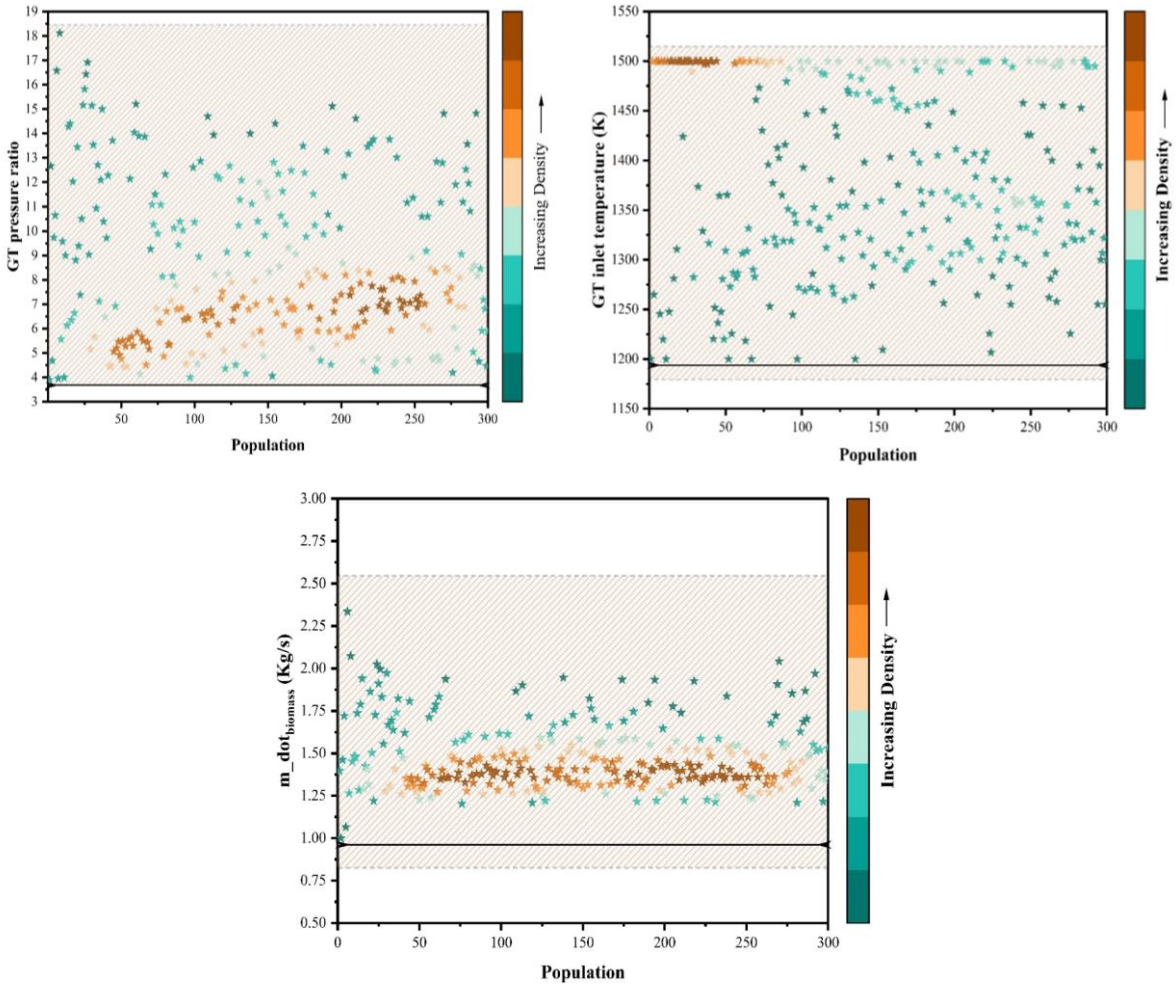

Fig. 14(a-c). A random distribution graph presenting the relationship between the GT pressure ratio, GTIT, and biomass flow rate for the first case.

6. Conclusions

This study introduces an innovative multigeneration facility that prioritizes the utilization of municipal solid waste as its primary fuel source. The plant incorporates advanced technologies, including a digester, organic Rankine cycle, MED, proton exchange membrane, and methanation. The primary function of this cogeneration system involves the conversion of hydrogen derived from PEM and CO_2 obtained through CO_2 capture into methane, while also generating distilled water or fresh water through heat recovery. The entire system has undergone thorough investigation from various perspectives, including environmental, energy, exergy, and exergoeconomic aspects. In addition, a thorough parametric study was conducted to assess the performance of the system across different operating conditions. The findings can be summarized below:

- With a second-law thermodynamics efficiency of 32.07%, the system demonstrates a noteworthy CO_2 emission index of 0.1649 kg/kWh and total cost products of 12.91 $\$/GJ$.
- This research demonstrates that allocating resources towards technology aimed at optimizing MED unit effects has the potential to enhance water production. These findings are vital for nations with limited water resources and might contribute to the development of effective and environmentally-friendly desalination technologies.
- The parametric research on Turbine Inlet Temperature (GTIT) demonstrates that changes in T_4 (ranging from 1150 to 1550 K) result in a 3.90% improvement in exergetic efficiency, accompanied by a reverse U-shaped unit cost pattern. Simultaneously, there is a linear decrease in specific CO_2 emissions as T_4 increases, resulting in a reduction of 9.95%. This highlights the intricate relationship among efficiency, cost, emissions, and turbine intake temperature.
- The system undergoes multi-objective optimization.
- The system attains a second law efficiency of 37.53%, a total cost of products of 8.402 $\$/GJ$, and a CO_2 emission index of 0.0134 kg/kWh in the multi-criteria optimization scenario.

The results show that this system has advantages for the economy and the environment, and it also follows the second rule of thermodynamics, which makes it cost-effective.

References

[1] Ameri M, Ahmadi P, Hamidi A. Energy, exergy, and exergoeconomic analysis of a steam power plant: A case study. Energy. 2009;34(5):499-512. https://doi.org/10.1002/er.

[2] Hossein M, Chitgar N, Ali M, Ahmadi P, Rosen MA. Performance assessment and optimization of a biomass-based solid oxide fuel cell and micro gas turbine system integrated with an organic Rankine cycle. Int J Hydrogen Energy. 2019;44(36):19931-19940. https://doi.org/10.1016/j.ijhydene.2019.12.143.

[3] Lillo P, Ferrer-Marti L, Fernández-Baldor Á, Ramírez B. A new integral management model and evaluation method to enhance sustainability of renewable energy projects for energy and sanitation services. Energy Sustain Dev. 2015;29:1-12. https://doi.org/10.1016/j.esd.2015.08.003.

[4] Kim YM, Sohn JL, Yoon ES. Supercritical CO2 Rankine cycles for waste heat recovery from gas turbine. Energy. 2017;118:893-905. https://doi.org/10.1016/j.energy.2016.10.106.

[5] Ghasemzadeh N, Ghiami Sardroud R, Gholamian E, Yari M. Comprehensive performance evaluation and multi-criteria optimization of a novel tri-generation system based on geothermal energy. Energy Equip Syst. 2024;12(1):29-45. https://doi.org/10.22059/ees.2023.2006891.1437.

[6] Salman CA, Schwede S, Naqvi M, Thorin E, Yan J. Synergistic combination of pyrolysis, anaerobic digestion, and CHP plants. Energy Procedia. 2019;158:1323-1329. https://doi.org/10.1016/j.egypro.2019.01.326.

[7] Zhang L, Sobhani B. Comprehensive economic analysis and multi-objective

optimization of an integrated power and freshwater generation cycle based on flash-binary geothermal and gas turbine cycles. J Clean Prod. 2022;364:132644. https://doi.org/10.1016/j.jclepro.2022.132644.

[8] Zeinali M, Sharifi A, Ranjbar F. Thermodynamic analysis of sustainable electric power production using solar tower during day and syngas combustion from municipal waste gasification during night. Energy Equip Syst. 2023;11(2):277-304. https://doi.org/10.22059/ees.2023.1999210.1421.

[9] Behzadi A, Gholamian E, Houshfar E, Ashjaee M, Habibollahzade A. Thermoeconomic analysis of a hybrid PVT solar system integrated with double effect absorption chiller for cooling/hydrogen production. Energy Equip Syst. 2018;6(4):413-427. https://doi.org/10.22059/ees.2018.33319.

[10] Ni M, Leung MKH, Leung DYC. Energy and exergy analysis of hydrogen production by a proton exchange membrane (PEM) electrolyzer plant. Energy Convers Manag. 2008;49(10):2748-2756. https://doi.org/10.1016/j.enconman.2008.03.018.

[11] Bailera M, Espatolero S, Lisbona P, Romeo LM. Power to gas-electrochemical industry hybrid systems: A case study. Appl Energy. 2017;202:435-446. https://doi.org/10.1016/j.apenergy.2017.05.177.

[12] Desideri U, Paolucci A. Performance modelling of a carbon dioxide removal system for power plants. Energy Convers Manag. 1999;40(20):1899-1915. https://doi.org/10.1016/S0196.8904(99)00074-6.

[13] Bailera M, Kezibri N, Romeo LM, Espatolero S, Lisbona P, Bouallou C. Future applications of hydrogen production and CO2 utilization for energy storage: Hybrid Power to Gas-Oxycombustion power plants. Int J Hydrogen Energy. 2017;42(22):13625-13632. https://doi.org/10.1016/j.ijhydene.2017.02.123.

[14] Ashour MM. Steady state analysis of the Tripoli West LT-HT-MED plant. L Energy. 2002;152:191-194.

[15] Khanmohammadi S, Kizilkan O, Nguyen DD. Simulation and exergy evaluation of a MED unit based on waste heat recovery from a gas turbine unit. Energy Equip Syst. 2022;10(4):229-239. https://doi.org/10.22059/ees.2022.254619.

[16] Montazerinejad H, Fakhimi E, Ghandehariun S, Ahmadi P. Advanced exergy analysis of a PEM fuel cell with hydrogen energy storage integrated with organic Rankine cycle for electricity generation. Sustain Energy Technol Assessments. 2022;51:101885. https://doi.org/10.1016/j.seta.2021.101885.

[17] Mofrad KG, Zandi S, Salehi G. Exergoeconomic and exergoenvironmental assessment of a geothermal-driven cogeneration system utilizing dual-pressure organic Rankine cycle and zeotropic mixtures. Energy Reports. 2023;9:5206-523. https://doi.org/10.1016/j.egyr.2023.04.271.

[18] Shamsi M, Moghaddas S, Torabi O, Bakhshehshi S, Bonyadi M. Design and analysis of a novel structure for green syngas and power cogeneration based on PEM electrolyzer and Allam cycle. Int J Hydrogen Energy. 2023;48(42):29034-29047. https://doi.org/10.1016/j.ijhydene.2023.04.069.

[19] Assareh E, Asl SSM, Agarwal N, Ahmadinejad M, Jalali A, Lee M. A Cogeneration-Coupled energy storage system utilizing hydrogen and methane-fueled CAES and ORC with ambient temperature consideration enhanced by artificial neural Network, and Multi-Objective optimization. Therm Sci Eng Prog. 2023;46:102161. https://doi.org/10.1016/j.tsep.2023.102161.

[20] Behzadi A, Gholamian E, Mojtaba S, Nourozi B. A comparative evaluation of alternative optimization strategies for a novel heliostat-driven hydrogen production/injection system coupled with a vanadium chlorine cycle. Energy Convers Manag. 2022;267:115878. https://doi.org/10.1016/j.enconman.2022.115878.

[21] Javaherian A, Yari M, Gholamian E, Carton JG, Mehr AS. Proposal and comprehensive analysis of power and green

hydrogen production using a novel integration of flame-assisted fuel cell system and Vanadium-Chlorine cycle: An application of multi-objective optimization. Energy Convers Manag. 2023;277:116659. https://doi.org/10.1016/j.enconman.2023.116659.

[22] Nami H, Mahmoudi SMS, Nemati A. Exergy, economic and environmental impact assessment and optimization of a novel cogeneration system including a gas turbine, a supercritical CO2 and an organic Rankine cycle (GT-HRSG/SCO2). Appl Therm Eng. 2017;110:1315-1330. https://doi.org/10.1016/j.applthermaleng.2016.08.197.

[23] Ahmadi S, Ghaebi H, Shokri A. A comprehensive thermodynamic analysis of a novel CHP system based on SOFC and APC cycles. Energy. 2019;186:115899. https://doi.org/10.1016/j.energy.2019.115899.

[24] Hamrang F, Shokri A, Seyed Mahmoudi SM, Ehghaghi B, Rosen MA. Performance analysis of a new electricity and freshwater production system based on an integrated gasification combined cycle and multi-effect desalination. Sustain. 2020;12(19):7996. https://doi.org/10.3390/su12197996.

[25] Dou Z, Zou Y, Mohebbi A. Design and multi-aspect analysis of a geothermal and biomass dual-source power, cooling, heating, and hybrid freshwater production system. Energy. 2024;293:130532. https://doi.org/10.1016/j.energy.2024.130532.

[26] Alotaibi S, Ibrahim OM, Luo S, Luo T. Modeling of a continuous water desalination process using directional solvent extraction. Desalination. 2017;420:114-124. https://doi.org/10.1016/j.desal.2017.07.00

[27] Balafkandeh A, Demirkan I. Advanced exergy analysis of a triple effect distillation unit integrated with CO2-based membrane separators. J Therm Sci Eng Appl. 2018;10(3):031010. https://doi.org/10.1115/1.4041645.

[28] Mostafavi Sani M, Noorpoor A, Shafie-Pour Motlagh M. Optimal model development of energy hub to supply water, heating and electrical demands of a cement factory. Energy. 2019;177:574–92. doi: 10.1016/j.energy.2019.03.043.

[29] Hesari F, Salimnezhad F, Khoshgoftar Manesh MH, Morad MR. A novel configuration for low-grade heat-driven desalination based on cascade MED. Energy. 2021;229:120657. https://doi.org/10.1016/j.energy.2021.120657.

[30] Khaleghi S, Asiaei S, Siavashi M. A smart grid poly-generation design for hot arid regions composed of multi-effect distillation (MED), compressed air energy storage (CAES), and parabolic trough solar collector field (PTSC). J Clean Prod. 2022;372:133693. https://doi.org/10.1016/j.jclepro.2022.133693.

[31] Clausen LR, Butera G, Jensen SH. Integration of anaerobic digestion with thermal gasification and pressurized solid oxide electrolysis cells for high efficiency bio-SNG production. Energy. 2019;188:116018. https://doi.org/10.1016/j.energy.2019.116018.

[32] Gao J, Wang Y, Ping Y, Hu D, Xu G, Gu F, et al. A thermodynamic analysis of methanation reactions of carbon oxides for the production of synthetic natural gas. RSC Adv. 2012;2:2358–68. https://doi.org/10.1039/c2ra00632d.

[33] Leveni M, Cozzolino R. Energy, exergy, and cost comparison of Goswami cycle and cascade organic Rankine cycle/absorption chiller system for geothermal application. Energy Convers Manag. 2021;227:113598.

[34] Esfandi S, Baloochzadeh S, Asayesh M, Ehyaei MA, Ahmadi A, Rabanian AA, et al. Energy, exergy, economic, and exergoenvironmental analyses of a novel hybrid system to produce electricity, cooling, and syngas. Energies. 2020;13:6453.

[35] Tayefeh M. Exergy and economic analysis of a novel integration of compressed air energy storage with multi-effect distillation and multi-stage flash systems. J Energy Storage. 2022;55:105534. https://doi.org/10.1016/j.est.2022.105534.

[36] Bejan A, Tsatsaronis G, Moran MJ. Thermal design and optimization. 1st ed. John Wiley & Sons; 1995.

[37] Wang S, Zhang L, Liu C, Liu Z, Lan S, Li Q, et al. Techno-economic-environmental evaluation of a combined cooling heating and power system for gas turbine waste heat recovery. Energy. 2021;231:120956.

[38] Ioroi T, Yasuda K, Siroma Z, Fujiwara N, Miyazaki Y. Thin film electrocatalyst layer for unitized regenerative polymer electrolyte fuel cells. J Power Sources. 2002;112:583–7. https://doi.org/10.1016/S0378.7753(02)00466-4.

[39] Bailera M, Lisbona P, Romeo LM. Avoidance of partial load operation at coal-fired power plants by storing nuclear power through power to gas. Int J Hydrogen Energy. 2019;44:26063–75. https://doi.org/10.1016/j.ijhydene.2019.08.033.

[40] Fakhari I, Behzadi A, Gholamian E, Ahmadi P, Arabkoohsar A. Design and tri-objective optimization of a hybrid efficient energy system for tri-generation, based on PEM fuel cell and MED using syngas as a fuel. J Clean Prod. 2021;290:125205. https://doi.org/10.1016/j.jclepro.2020.125205.